RSC Advances

PAPER

View Article Online
View Journal | View Issue

Cite this: *RSC Adv.*, 2024, **14**, 36970

Production of aromatic hydrocarbons from catalytic fast pyrolysis of microalgae over Fe-modified HZSM-5 catalysts

Xinyun Wang, *[a] Chuan Li,[a] Jiliang Yang,[a] Yefeng Liu,[a] Jinpei Hei,[a] Shiqi Huang[b] and Daming Gao[b]

In this study, catalytic fast pyrolysis of the microalga *C. pyrenoidosa* over Fe-modified HZSM-5 catalysts was performed to produce aromatic hydrocarbons using analytical pyrolysis-gas chromatography/mass spectrometry (Py-GC/MS). Fe-modified HZSM-5 catalysts were prepared using wet impregnation and characterized through X-ray diffraction (XRD), scanning electron microscopy (SEM), N_2 adsorption–desorption and temperature-programmed desorption of ammonia (NH_3-TPD) analysis. The effect of Fe loading (3, 5, 8, and 12 wt%) and pyrolysis temperature (450, 500, 550, 600 °C) on the content of pyrolysis products and the content and selectivity of aromatics was examined. Results showed that the parent HZSM-5 catalyst structure remained intact upon increasing Fe loading, although its specific surface area, micropore volume and average pore diameter decreased. In addition, its external specific surface area and total pore volume increased. The modification of Fe metal increased the total acid amount, especially strong acid sites, which were highest when Fe loading was 8 wt%. The prepared Fe-modified HZSM-5 catalysts exhibited pronounced deoxygenation and denitrogenation effects, which significantly decreased the acid, aldehyde, ketone, furan and nitrogenous compounds, thus improving the production of monocyclic aromatic hydrocarbons (MAHs) while effectively suppressing the formation of polycyclic aromatic hydrocarbons (PAHs). The highest content of aromatic hydrocarbons was obtained with an Fe loading of 8 wt% and pyrolysis temperature of 500 °C, which was 42.5%. As Fe loading increased, benzene selectivity decreased, while the selectivity of toluene and xylene first increased and then decreased. With an increase in pyrolysis temperature, benzene selectivity increased, whereas toluene and xylene selectivity increased at first and then decreased. Reaction mechanisms for the formation of aromatic hydrocarbons during the catalytic pyrolysis of microalgae are put forward. This research revealed that catalytic fast pyrolysis of microalgae over Fe-modified HZSM-5 catalysts is an effective method to produce MAHs.

Received 21st September 2024
Accepted 3rd November 2024

DOI: 10.1039/d4ra06815g

rsc.li/rsc-advances

1. Introduction

Aromatic hydrocarbons, in particular, MAHs such as benzene, toluene and xylene (BTX), are important platform chemicals in the petrochemical industry and are widely used as gasoline fuel additives and chemical feedstocks for producing plastics, synthetic fibers and medicines.[1] Aromatic hydrocarbons are traditionally derived from petroleum. Considering the rapid depletion of fossil fuels and increasing environmental problems, producing aromatic hydrocarbons from renewable and environmentally friendly biomass resources has attracted increasing attention worldwide.[2] Biomass energy resources, mainly including lignocellulosic and algal biomasses, are abundant on the earth.[3] Algal biomass mainly consists of proteins, lipids and carbohydrates, which are easy to be pyrolyzed compared with lignocellulosic biomass, which is mainly composed of cellulose, hemicellulose and lignin. Algal biomass has been considered one of the most potential biomass energy sources for third-generation biofuels and high value-added chemicals. Microalgae have received growing interest recently as a source for biofuel production because of their fast growth rate, no competition for arable land and high carbon sequestration efficiency.[4]

Catalytic fast pyrolysis (CFP) is a promising technology that can directly convert biomass feedstocks into valuable aromatics because of the green and sustainable characteristics of biomass. Among various catalysts, HZSM-5 zeolite is the most widely used catalyst owing to its moderate pore structure, strong acidity, and high hydrothermal stability.[5] The HZSM-5 zeolite catalyst has shown a significant effect in reducing oxygenated compounds or nitrogenous compounds and increasing the production of

[a]*School of Chemistry and Materials Engineering, Chaohu University, Chaohu 238024, China. E-mail: 053021@chu.edu.cn*
[b]*School of Energy Materials and Chemical Engineering, Hefei University, Hefei 230601, China*

aromatic hydrocarbons from pyrolysis of biomass.[6–15] However, HZSM-5 zeolite is easily and rapidly deactivated during the catalytic pyrolysis process of biomass due to the formation of coke on the catalyst surface, which results in a decrease in the catalytic activity and yield of aromatic hydrocarbons, thus restricting the conversion of aromatics.[16]

Metal-modified HZSM-5 is effective as it tunes the channel and acid active sites of the catalyst to relieve catalyst deactivation and improve the aromatics yield in the CFP of biomass. Previous studies have shown that the impregnation of certain metals (Ni, Co, Ga, La, Zr, Ce, Mg, Cu, Zn, Fe) into HZSM-5 can enhance the production of aromatic hydrocarbons and reduce the amount of oxygenated compounds in bio-oil as well as coke formation.[16–27] Among these selected metals, Fe is one of the most commonly used metals for the production of aromatic hydrocarbons from the catalytic pyrolysis of lignocellulosic biomass.[16,20,21,26,27] Moreover, Fe is cheaper compared other metals. Mullen *et al.* studied the production of aromatic hydrocarbons from the catalytic pyrolysis of biomass over different Fe-loaded modified HZSM-5. Results showed that 1.4 wt% Fe/HZSM-5 produced the highest increase in the production of MAHs from the catalytic pyrolysis of cellulose, cellobiose and lignin.[16] Sun *et al.* investigated the catalytic fast pyrolysis of poplar sawdust over Fe-modified ZSM 5 catalysts to produce MAHs and found that the 15 wt% Fe/ZSM-5 catalyst displayed the highest yield of MAHs, indicating that the coordination effect between Fe metal active sites and ZSM-5 acid sites promoted the production of MAHs and hindered the formation of PAHs.[20] Chai *et al.* reported that Fe-modified ZSM-5 can increase the yield of aromatics from the catalytic pyrolysis of corn stalk, and the incorporation of Fe into ZSM-5 increased the yield of MAHs and decreased the yield of PAHs.[21]

As reviewed above, although several studies have been conducted on the production of aromatic hydrocarbons from the catalytic fast pyrolysis of lignocellulosic biomass over Fe-modified HZSM-5 catalysts, which exhibited excellent catalytic performance and significantly enhanced the yield of MAHs and suppressed the formation of PAHs, there are few studies on microalgae pyrolysis using transition metal Ni-loaded HZSM5catalysts,[28,29] suggesting that the addition of Ni metal increased the catalytic activity for the aromatization of HZSM-5 and significantly promoted the deoxidation, denitrification and aromatization to produce more aromatic hydrocarbons. To date, there is no literature on the catalytic fast pyrolysis of microalgae over Fe modified HZSM-5 catalysts for aromatics production.

Therefore, in order to evaluate the catalytic performance of Fe-modified HZSM-5 catalysts for the production of aromatic hydrocarbons from the catalytic pyrolysis of microalgae, this work conducted the fast catalytic pyrolysis of microalgae *C. pyrenoidosa* over Fe-modified HZSM-5 catalysts prepared by the wet impregnation method and characterized by XRD, SEM, N_2 adsorption–desorption and NH_3-TPD analyses using Py-GC/MS and systematically investigated the effect of Fe loading (3, 5, 8, 12 wt%) and pyrolysis temperature (450, 500, 550, 600 °C) on the content of pyrolysis products as well as the content and selectivity of aromatics. The reaction mechanisms of aromatic hydrocarbons' formation from the catalytic pyrolysis of microalgae were proposed. The study on the catalytically-oriented pyrolysis of microalgae for producing aromatic hydrocarbons is beneficial for theoretical reference and guidance for the high value-added utilization of microalgae.

2. Experimental

2.1 Materials

The feedstock of microalgae *C. pyrenoidosa* with a green food grade was provided by Wudi Lvqi Bioengineering Co. Ltd (Shangdong Province, China). The proximate analysis was performed according to the Chinese National Standard GB/T 28731-2012 to determine the contents of moisture (M), volatile matter (V) and ash (A), and the fixed carbon (FC) content was calculated by the difference. The elemental contents of C, H, N and S were determined by an elemental analyzer (Vario EL, Elementar, Germany). O content was calculated by the difference. The results of proximate analysis and ultimate analysis of the microalgae sample are presented in Table 1.

HZSM-5 zeolite catalyst with Si/Al ratio of 46 was purchased from the Catalyst Plant of Nankai University (Tianjin, China). $Fe(NO_3)_3 \cdot 9H_2O$ was purchased from Sinopharm Chemical Reagent Co., Ltd (Shanghai, China).

2.2 Catalyst preparation and characterization

Before the experiment, the original HZSM-5 powders were calcined in air at 550 °C for 4 h to obtain the parent HZSM-5 catalyst. The Fe-modified HZSM-5 zeolite catalysts were prepared by the wet impregnation method. In this work, Fe loading based on the mass ratio of Fe metal to parent HZSM-5 was 3, 5, 8, 12 wt% and the corresponding catalysts were denoted as 3Fe/HZSM-5, 5Fe/HZSM-5, 8Fe/HZSM-5 and 12Fe/HZSM-5, respectively. The preparation procedure of the Fe-modified HZSM-5 catalyst is as follows: a certain amount of $Fe(NO_3)_3 \cdot 9H_2O$ weighed was dissolved into 100 mL deionized water to prepare the aqueous solution, and then 10 g of the parent HZSM-5 was added and magnetically stirred at 80 °C for 4 h. After that, the mixture was dried at 105 °C for 12 h. Lastly, the obtained cake was calcined at 550 °C for 4 h in an ambient atmosphere and pulverized and sieved by passing through an 80-mesh screen after cooling to obtain the 3Fe/HZSM-5, 5Fe/HZSM-5, 8Fe/HZSM-5 and 12Fe/HZSM-5 catalyst. The preparation processes of Fe-modified HZSM-5 catalysts are illustrated in Fig. 1.

The phase structure of the parent and Fe-modified HZSM-5 catalysts was characterized by powder X-ray diffraction (XRD) on an X-ray diffractometer (D/MAX-2500PC, Rigaku, Japan) with CuKα ($\lambda = 1.5406$ nm) radiation and operating at 40 kV and 40 mA. The scanning rate was set at 5° min^{-1} in the 2θ range of 5°–

Table 1 The proximate and ultimate analyses of *C. pyrenoidosa*

Proximate analysis[a] (wt%)				Ultimate analysis[b] (wt%)				
M	V	A	FC	C	H	N	S	O
6.62	70.41	6.28	16.69	47.28	7.38	8.45	0.82	29.79

[a] Air dry basis. [b] Dry ash-free basis.

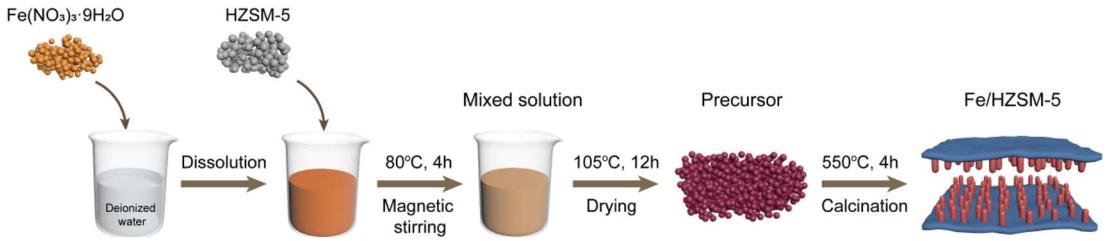

Fig. 1 Preparation processes of Fe-modified HZSM-5 catalysts.

80°. The morphology of the parent and Fe-modified HZSM-5 catalysts were analyzed by scanning electron microscopy (SEM) on a field-emission scanning electron microscope (Quanta 450 FEG, FEI Company, USA). The textural property of the parent and Fe-modified HZSM-5 catalysts were measured by N_2 adsorption and desorption isotherms on an automatic specific surface area and aperture analyzer (Autosorb-IQ3, Quantachrome Instrument, UAS). The samples were degassed for 8 h under N_2 at 300 °C prior to the measurements. The N_2 adsorption–desorption experiments were conducted at −196 °C. The multipoint Brunauer–Emmett–Teller (BET) method was used to calculate the specific surface area (S_{BET}). The micropore specific surface area (S_{micro}) and volume (V_{micro}) were determined by the t-plot method, while the external specific surface area ($S_{external}$) was calculated by difference. The total pore volume (V_{total}) was derived from the amount of N_2 adsorbed at $p/p_0 = 0.9$. The average pore diameter ($D_{average}$) was obtained from the adsorption branch of the isotherm using the Barrett–Joyner–Halenda (BJH) method. The acidity of the catalysts was estimated by the temperature-programmed desorption of NH_3 (NH_3-TPD) on a chemisorption instrument (AutoChem II 2920, Micromeritics Instrument Corporation, USA) equipped with a thermal conductivity detector (TCD). The sample was degassed at 400 °C and an He flow rate of 50 mL min^{-1} for 1 h. After pretreatment, the sample was cooled to ambient temperature and saturated with NH_3 gas in 10% NH_3/He for 1 h. The physically absorbed NH_3 was then blown out at an He flow rate of 50 mL min^{-1} for 1 h. The temperature was raised from 50 °C to 600 °C at a heating rate of 10°C min^{-1}. The NH_3-TPD signal was recorded by a thermal conductivity detector (TCD).

2.3 Catalytic fast pyrolysis by Py-GC/MS

Py-GC/MS experiments were carried out using an analytical pyrolyzer (EGA/EY3030D, Frontier Laboratories, Japan) coupled with gas chromatograph-mass spectrometer (GCMS-2010, Shimadzu, Japan). 0.5% ± 2% mg sample (microalgae, even a mixture of microalgae and catalyst with a mass ratio of 1 : 5) was wrapped in a ferromagnetic foil and pyrolyzed in each experiment. The experiments were performed at different temperatures (450–600 °C) for 10 s with a heating rate of 20 °C ms^{-1}. The separation analysis of the volatile products was performed using an Agilent DB-5MS capillary column (30 m length × 0.25 mm inner diameter × 0.25 μm film thickness). High purity (99.999%) helium (He) was used as the carrier gas with a flow rate of 1.0 mL min^{-1}. The temperature of the injector was kept at 270 °C with a split ratio of 60 : 1. The temperature of the transfer line was set at 280 °C. The initial oven temperature was set at 40 °C and maintained for 2 min and raised with a heating rate of 10 °C min^{-1} to 300 °C and held for 2 min. MS was operated in the electron ionization (EI) mode in the range of 50–400 m/z at an ionization voltage of 70 eV. The ion source temperature was kept at 260 °C. The pyrolysis vapour products were identified by comparison with the National Institute of Standards and Technology (NIST) mass spectral data library.

Since the relative content of each component in the pyrolysis vapour products is proportional to the chromatographic peak area, the relative content of each composition was determined by calculating the chromatographic area percentage. The selectivity of a specific identified aromatic hydrocarbons was calculated as follows.

$$S = \frac{R}{\sum R} \quad (1)$$

where S is the selectivity of a certain kind of aromatic hydrocarbons, such as benzene, toluene, xylene and naphthalene, R is the relative content of a specific identified aromatic hydrocarbons, and $\sum R$ is the total relative content of all aromatic hydrocarbons.

3. Results and discussion

3.1 Characterization of the catalyst

The XRD patterns of the parent HZSM-5 and Fe-modified HZSM-5 catalysts are shown in Fig. 2.

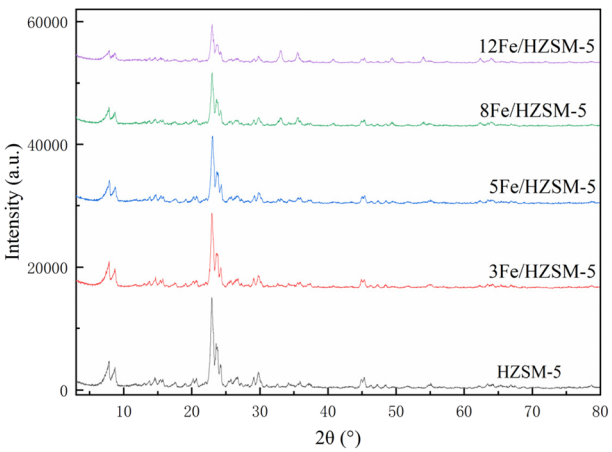

Fig. 2 XRD patterns of the parent HZSM-5 and Fe-modified HZSM-5 catalysts.

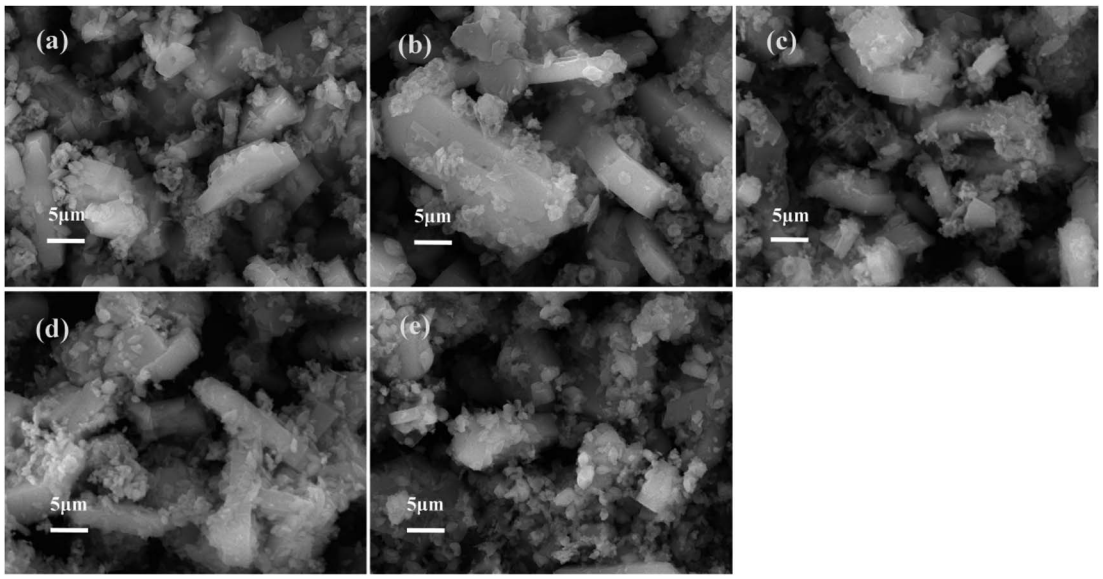

Fig. 3 SEM micrographs of the catalyst: (a) parent HZSM-5, (b) 3Fe/HZSM-5, (c) 5Fe/HZSM-5, (d) 8Fe/HZSM-5, and (e) 12Fe/HZSM-5.

It is apparent that the patterns of all the catalysts were consistent with the MFI structure of the HZSM-5 parent, with characteristic diffraction peaks observed at $2\theta = 7.8$, 8.8, 9.0, 13.8, 14.7, 23.2, 23.6, and 29.9°, which indicates that the modification of Fe metal does not change the structure of the HZSM-5 parent catalyst. It can be seen that there is no characteristic diffraction peaks of the Fe oxide crystals shown in the XRD patterns of the Fe-modified HZSM-5 catalysts, indicating that the Fe metal oxides are more evenly dispersed on the external surface of the HZSM-5.[30] However, for the Fe-modified HZSM-5, the intensities of the characteristic peaks of HZSM-5 decreased. Moreover, with an increasing Fe loading, the intensities of the characteristic peaks of HZSM-5 decreased continuously, which is consistent with the previous literature reports.[31,32] This result can be attributed to Fe ions, which could enter into the framework structure of HZSM-5 well, resulting in the reduction of the crystallinity of the HZSM-5 catalyst support.

The SEM micrographs of the parent HZSM-5 and Fe-modified HZSM-5 catalysts are shown in Fig. 3. As can be seen, the morphology of the Fe-modified HZSM-5 is similar to that of the parent HZSM-5, which suggests that Fe metal oxide particles are also uniformly dispersed on the HZSM-5 support, which is in accordance with the abovementioned XRD analysis results.

The N_2 adsorption–desorption isotherms and the corresponding pore dimeter distributions of different catalysts are illustrated in Fig. 4, and the textural properties of the HZSM-5 parent and Fe-modified HZSM-5 catalysts are listed in Table 2.

As shown in Fig. 4(a), the parent HZSM-5 and Fe-modified HZSM-5 catalysts showed type IV isotherms with remarkable hysteresis loops appearing at higher relative pressures. Fig. 4(b) shows that the pore diameter distribution was found centered at approximately 3–6 nm. As it can be seen from Table 2, the impregnation of Fe metal decreased the S_{BET}, S_{micro}, V_{micro} and $D_{average}$ of the Fe-modified HZSM-5 because that the Fe oxides were adsorbed in the HZSM-5 surface or enter into the channels, thus blocking the pore channel. However, the $S_{external}$ and V_{total} of the Fe-modified HZSM-5 increased. This phenomenon

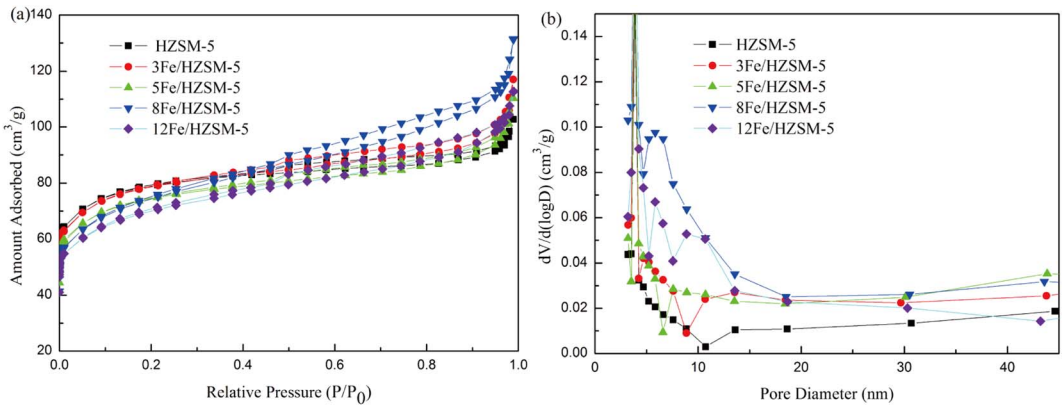

Fig. 4 Pore structure parameters of catalysts: (a) N_2 adsorption–desorption isotherms and (b) pore diameter distributions.

Table 2 Textural and porous properties of the catalysts

Catalyst	S_{BET} (m^2 g^{-1})	S_{micro} (m^2 g^{-1})	V_{total} (cm^3 g^{-1})	$V_{micro\backslash}$ (cm^3 g^{-1})	$D_{average}$ (nm)
HZSM-5	295.446	253.499	0.1588	0.104	3.865
3Fe/HZSM-5	291.625	241.470	0.1809	0.100	3.862
5Fe/HZSM-5	275.599	226.011	0.1707	0.094	3.860
8Fe/HZSM-5	268.248	176.107	0.2033	0.076	3.856
12Fe/HZSM-5	254.109	181.572	0.1745	0.077	3.859

can be attributed to the formation of oligomeric Fe_xO_y clusters on the catalyst surface, which may promote the increase in mesopores,[33] resulting in the increase in $S_{external}$ and V_{total}. In summary, catalysts modified by Fe metal can decrease the surface area, micropore volume and average pore size but increase the external surface area. These indicate that the incorporation of Fe metal plays a role in modifying the HZSM-5 catalyst surface and pore channel.

The NH_3-TPD results of parent HZSM-5 and Fe-modified HZSM-5 catalysts are presented in Fig. 5. As can be seen from Fig. 5, all the NH_3-TPD profiles exhibited two typical desorption peaks of ammonia located at about 120 °C and 400 °C. The desorption peak temperature represents the strength of the acid sites. The low peak temperature corresponds to the weak acid sites, which is related to the Lewis acid, while the high peak temperature corresponds to the strong acid sites, which is related to the Brønsted acid.[34] The peak area represents the acid amount, and the smaller peak area is less than the larger peak area.[34]

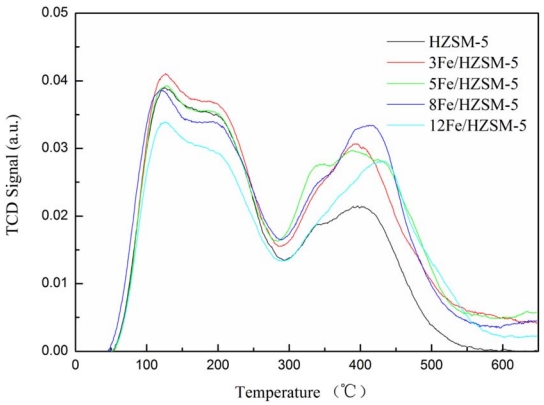

Fig. 5 NH_3-TPD of the parent HZSM-5 and Fe-modified HZSM-5 catalysts.

The peak temperature and acid amount of the all catalysts are listed in Table 3. In comparison with parent HZSM-5, the strength and amount of weak acid sites of Fe-modified HZSM-5 showed almost no change except for a decrease for 12Fe/HZSM-5, while the strength and amount of strong acid sites increased significantly. When the Fe loading reached 8 wt%, the amount of strong acid sites was the maximum, and when the Fe loading further increased, it then decreased. Furthermore, the amount of total acid of Fe-modified HZSM-5 increased significantly, which reached the maximum with increasing Fe loading up to 8 wt%. On further increasing the Fe loading, the total acid amount of Fe-modified HZSM-5 showed less improvement compared with that of the parent HZSM-5, which is in agreement with the previous results.[35,36] This may be because the higher Fe loading made Fe ion replace H^+ on the HZSM-5 surface, thus reducing its acid amount.[37]

The above characterization results of catalysts show that the addition of metal Fe to HZSM-5 zeolite modifies its textural and acid properties and improves the strong acid sites and the total amount of the catalyst, which lead to a high yield of aromatic hydrocarbons.[38]

3.2 Effect of Fe loading

Fe loading plays an important role in the formation of aromatic hydrocarbons. Thus, in this study, the catalytic pyrolysis experiments of microalgae were performed with different Fe loadings (3, 5, 8, 12 wt%) at a pyrolysis temperature of 500 °C. The effect of Fe loading on the content of pyrolysis products and the content and selectivity of aromatic hydrocarbons were investigated.

3.2.1 Effect of Fe loading on the content of pyrolysis products. The content of pyrolysis products with different Fe loadings is shown in Fig. 6. Pyrolysis products from microalgae are a very complex product containing a mixture of organic compounds, such as oxygen-containing compounds of

Table 3 Peak temperatures and acid amount of the catalysts

	Weak acid		Strong acid		
Catalyst	Peak temperature (°C)	Acid amount (mmol g^{-1})	Peak temperature (°C)	Acid amount (mmol g^{-1})	Total amount (mmol g^{-1})
HZSM-5	124.3	0.56	395.6	0.31	0.87
3Fe/HZSM-5	126.4	0.59	391.2	0.41	1.00
5Fe/HZSM-5	127.1	0.57	389	0.42	0.99
8Fe/HZSM-5	120	0.56	412	0.46	1.02
12Fe/HZSM-5	126.3	0.49	431.3	0.39	0.88

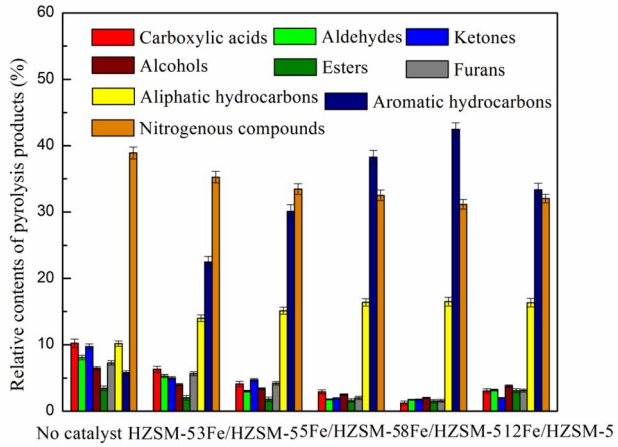

Fig. 6 Pyrolysis product content with different Fe loading.

aldehydes, ketones, alcohols, esters, carboxylic acids and furans, nitrogen-containing compounds of amides, amines nitriles and N-heterocyclic compounds, as well as hydrocarbons. Pyrolysis products can be divided into nine categories, such as acids, aldehydes, ketones, alcohols, esters, furans, aliphatic hydrocarbons, aromatic hydrocarbons and nitrogenous compounds.

It was found from Fig. 6 that the main pyrolysis products with no catalyst were oxygenated compounds (45.1%), followed by nitrogenous compounds (38.9%) and aliphatic hydrocarbons (10.2%), with relatively few aromatic hydrocarbons, accounting for only 5.8%. With the addition of the parent HZSM-5 catalyst, the content of acids, aldehydes, ketones and furans significantly decreased, while that of nitrogenous compounds decreased to a certain extent. At the same time, the aromatic hydrocarbons significantly increased up to 22.5%. The results indicate that the HZSM-5 catalyst has good deoxygenation and limited denitrification effects. In general, HZSM-5 zeolite possesses a large number of acid sites, significantly promoting the deoxygenation by H_2O, CO, CO_2, cracking, alkylation, cyclization and aromatization of oxygenated pyrolysis vapors and producing high aromatic hydrocarbons.[39,40] Meanwhile, HZSM-5 can promote nitrogen removal by NH_3 and HCN during the pyrolysis of nitrogenous compounds and promote the conversion of nitrogen-containing compounds derived from protein pyrolysis into aromatic hydrocarbons.[41,42]

Compared with the parent HZSM-5, the Fe-modified HZSM-5 catalysts showed more beneficial deoxygenation and denitrification effect and can better improve the production of aromatic hydrocarbons. The incorporation of Fe can significantly reduce the contents of acids, aldehydes, ketones, furans and nitrogen-containing compounds, resulting in an increase in the aromatic hydrocarbon content. As the Fe loading increased, the content of aromatic hydrocarbons increased and then decreased. The content of aromatic hydrocarbons was 30.1, 38.3, 42.5 and 33.3%, respectively, when the Fe loading was 3, 5, 8 and 12 wt%, respectively. The decrease in the aromatic hydrocarbons content is because the higher Fe metal loading reduces its amount of total acid and strong acid sites, decreasing its cracking and activity[43] and aromatic hydrocarbons content. The above results demonstrate that the combination of Fe and the acid sites of HZSM-5 allowed the oxygenated compounds of pyrolysis vapors to come into contact with the active sites on the surface and channels of the catalyst, resulting in the formation of aromatic hydrocarbons through a series of dehydration, cracking, decarboxylation, decarbonylation and oligomerization reactions, followed by cyclization and aromatization reactions.[44] The acidity of catalysts has been considered to play a vital role in the formation of aromatic hydrocarbons during catalytic pyrolysis.[44] On the one hand, Lewis acid sites play an important role in the dehydration reaction. On the other hand, Brønsted acid sites play a significant role in cracking, cyclization and aromatization reactions.[26] According the above NH_3-TPD analysis, Fe modification increases the strong acid sites and the total acid amount of the catalysts. As the Fe loading was 8 wt%, the total acid amount was maximized. Therefore, it can be concluded that the greater the total acid amount and the strong acid sites, the higher the content of aromatic hydrocarbons. This result is similar to the findings of the previous study.[16,18,31]

3.2.2 Effect of Fe loading on the content and selectivity of aromatics. The content of aromatic hydrocarbons from the catalytic pyrolysis of microalgae with different Fe loadings is given in Fig. 7. It can be seen that aromatic hydrocarbon product includes MAHs such as benzene, toluene and xylene. At the same time, it also contains a certain amount of PAHs, such as naphthalene, which promotes the formation of coke on the catalyst surface and leads to catalyst deactivation, resulting in a decrease in aromatic hydrocarbons production.[45] With the addition of Fe to HZSM-5 support, the benzene, toluene and xylene content increased, while the naphthalene content decreased. Fe metal enhances deoxygenation and hydrogenation by promoting hydrogen transfer reactions, which can restrain the secondary cyclization of MAHs, thus inhibiting the formation of PAHs, eventually leading to an increase in MAHs and a decrease in PAHs.[20,30] These indicate that Fe-modified HZSM-5 catalysts have excellent catalytic activity, which can

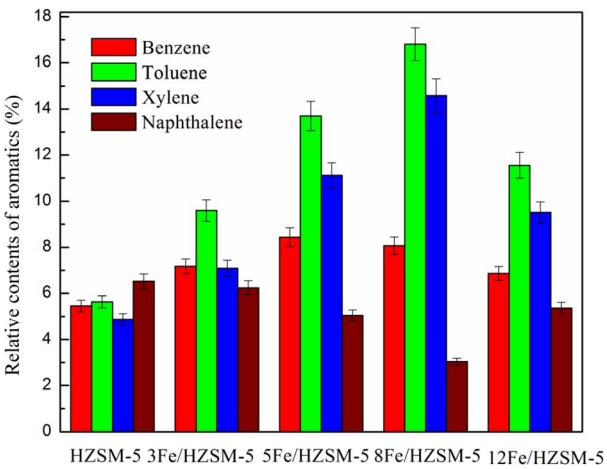

Fig. 7 Content of aromatics with different Fe loadings.

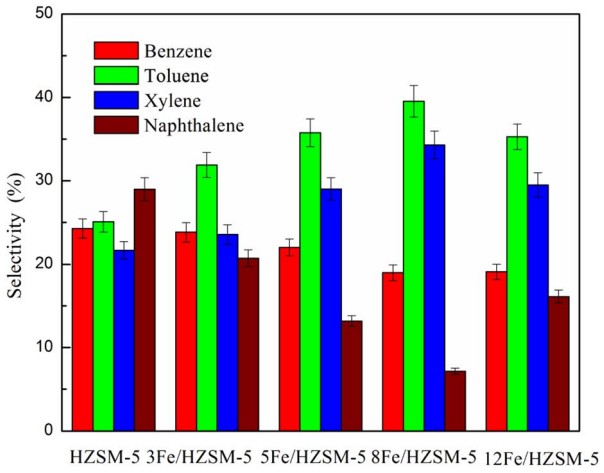

Fig. 8 Selectivity of aromatics with different Fe loadings.

enhance the production of MAHs and inhibit the formation of PAHs. Previous studies have also found that the addition of Ni and Fe into ZSM-5 can hinder the formation of PAHs, which produce lower PAHs compared to the parent ZSM-5 catalyst.[20,24] However, more Fe loading will increase the content of PAHs. At an Fe loading of 8 wt%, the BTX and naphthalene content reached the maximum value (39.5%) and the minimum value (3%), respectively.

The selectivity of aromatics composed of benzene, toluene, xylene and naphthalene is presented in Fig. 8. It can be seen that toluene has the highest selectivity among the benzene, toluene and xylene products, which indicates that HZSM-5 and Fe-modified HZSM-5 catalysts can significantly promote the production of toluene from microalgae pyrolysis. As shown in Fig. 8, it was also found that with an increase in Fe loading, benzene selectivity decreased, while toluene and xylene selectivity first increased and then decreased. When the Fe loading was 8 wt%, toluene and xylene selectivity was the maximum. This may be because the Fe-modified HZSM-5 catalyst promotes the alkylation of benzene.[31,46] Moreover, with increasing the Fe loading up to 8 wt%, the selectivity of naphthalene first decreased and then increased, which indicates that the high total acid amount inhibited the formation of PAHs.

3.3 Effect of pyrolysis temperature

In the study, the catalytic pyrolysis experiments of microalgae were conducted at different temperatures (450, 500, 550 and 600 °C) over 8Fe/HZM-5. The effect of pyrolysis temperature on the content of pyrolysis products and the content and selectivity of aromatic hydrocarbons were researched.

3.3.1 Effect of pyrolysis temperature on the content of pyrolysis products. The content of pyrolysis products at different temperatures is shown in Fig. 9. It can be observed that the contents of oxygen-containing compounds such as acids, aldehydes, ketones, furans and nitrogenous compounds significantly decreased with the increase in the temperature up to 500 °C, beyond which it increased. These indicate that the deoxygenation and denitrification effect of the Fe-modified HZSM-5 catalyst decreased at high temperature. The content

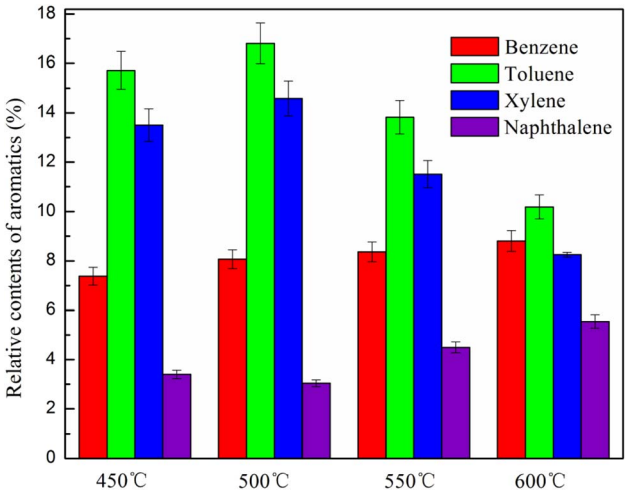

Fig. 10 Content of aromatics at different temperatures.

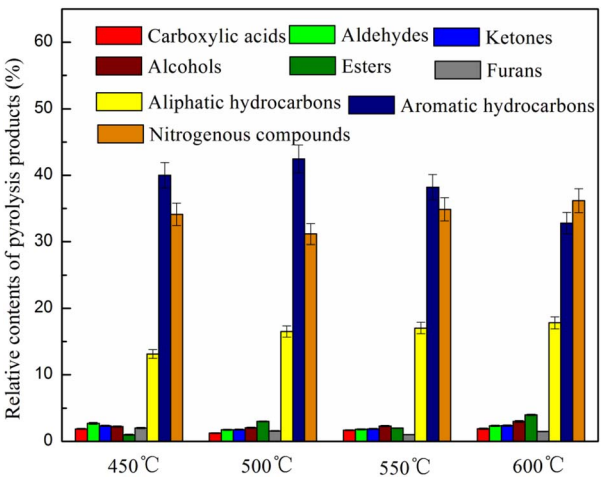

Fig. 9 Pyrolysis product content at different temperatures.

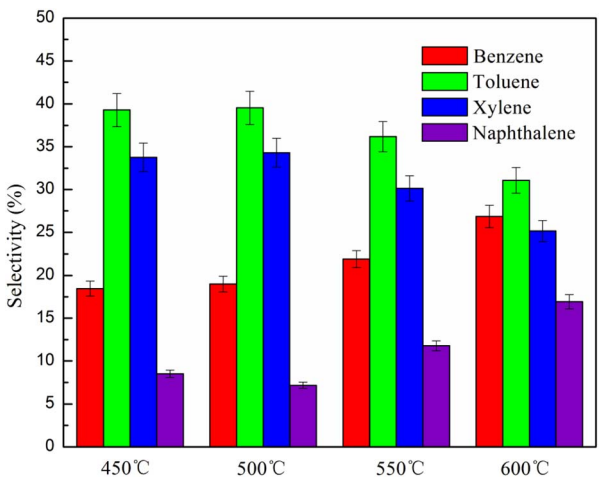

Fig. 11 Selectivity of aromatics at different temperatures.

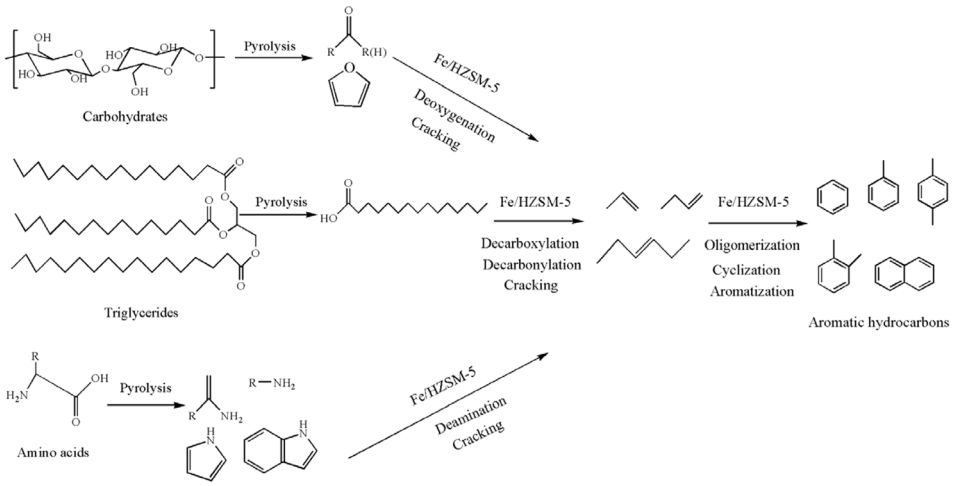

Fig. 12 Proposed reaction mechanisms for the formation of aromatic hydrocarbons from catalytic pyrolysis of microalgae.

of nitrogen-containing compounds increased with higher temperature (>500 °C), which is similar to that found in the literature.[29]

It can be seen that from Fig. 9 that the content of aromatic hydrocarbons significantly increased with the increase in the temperature up to 500 °C, after which it evidently decreases. When the pyrolysis temperature was 450, 500, 550 and 600 °C, the content of aromatic hydrocarbons was 40.1, 42.5, 38.2 and 32.6%, respectively. At low temperature, the pyrolysis reaction is not sufficient, resulting in less pyrolysis vapors; thus, the production of aromatic hydrocarbon is less. At high temperature, Fe-modified HZSM-5 catalyst can promote the deoxygenation and denitrogenation reaction of the pyrolysis vapors,[47] thus accelerating the formation of aromatic hydrocarbons. The decrease in aromatic hydrocarbons at higher temperatures of more than 500 °C is attributed to the significant secondary cracking of pyrolysis vapors and formation of gaseous products.[47]

3.3.2 Effect of pyrolysis temperature on the content and selectivity of aromatics. The content of aromatic hydrocarbons at different temperatures is given in Fig. 10. It was found that with increasing temperature, the content of MAHs increased at first and then decreased, while the content of PAHs initially decreased and then increased. The highest content of MAHs and the lowest content of PAHs were obtained at a pyrolysis temperature of 500 °C, which was 39.5% and 3%, respectively. PAHs generated from secondary reactions of benzene derivatives increased with an increase in the pyrolysis temperature. The high content of PAHs at a higher temperature (>500 °C) is similar to that reported in previous findings.[48]

The selectivity of aromatic hydrocarbons such as benzene, toluene, xylene and naphthalene is presented in Fig. 11. It can be seen that with increasing temperature, benzene selectivity increased, while toluene and xylene selectivity first increased and then decreased. At the same time, naphthalene selectivity first decreased and then increased. Benzene and toluene could be converted into xylene easily at low catalytic pyrolysis temperature because alkylation is an exothermic process;[22] thus, toluene selectivity increased before a pyrolysis temperature of 500 °C. At a high temperature of 600 °C, the degradation of monocyclic aromatic rings was promoted as well as their recombination to produce naphthalene. Thus, naphthalene selectivity increased, while that of toluene and xylene decreased.

3.4 Reaction mechanism for the formation of aromatic hydrocarbons

Microalgae catalytic pyrolysis has been carried out widely,[6–11] while the reaction mechanisms for aromatic hydrocarbon formation from microalgae still need further research. Generally, the major constituents of microalgae are carbohydrates, lipids and proteins.[49–51] Low-molecular weight oxygenated pyrolysis vapors, such as aldehydes, ketones and furans derived from carbohydrates composed of monosaccharides connected through glycosidic bonds, are deoxygenated and cracked into olefins.[11,52,53] Lipids are commonly triglycerides.[54] Triglycerides are thermally decomposed to heavy oxygenated hydrocarbons, such as long chain fatty acids, which undergo decarboxylation coupled with decarbonylation and are then cracked into olefins.[11,55] Proteins are made up of multiple amino acids connected by peptide bonds.[56] Nitrogenous organic compounds such as amides, amines and N-heterocyclic compounds derived from proteins pyrolysis through deamination are then cracked into olefins.[57] These olefins subsequently undergo a series of oligomerization, cyclization and aromatization reactions over Fe-modified HZSM-5 catalysts and are eventually converted to aromatic hydrocarbons.[11,52,53,55,57] Based on the literature and our results, the possible reaction pathways for aromatic hydrocarbon formation in the catalytic pyrolysis of microalgae are depicted in Fig. 12.

4. Conclusions

The production of aromatic hydrocarbons from the catalytic fast pyrolysis of microalgae over Fe-modified HZSM-5 catalysts was investigated by Py-GC/MS. Fe-modified HZSM-5 catalysts were

prepared by the wet impregnation method and were characterized by XRD, SEM, BET and NH_3-TPD analyses. Results showed that the addition of Fe metal resulted in changes in the physical structure of the parent HZSM-5 catalyst, including decreases in the intensity of the characteristic peak, specific surface area and average pore diameter and increases in the total acid amount, especially the strong acid sites. The highest content (39.5%) of MAHs and the lowest content (3%) of PAHs were obtained with Fe loading of 8 wt% and at a pyrolysis temperature of 500 °C. The existence of metal Fe on HZSM-5 led to an enhanced production of MAHs and a decreased production of PAHs. The aim of future research is to investigate the co-pyrolysis of microalgae and waste plastics over Fe-modified HZSM-5 catalysts in order to further improve the yield of MAHs, showing high potential for use as high value-added chemicals.

Data availability

The data associated with this article have been included in the manuscript.

Author contributions

Xinyun Wang: resources, supervision, project administration, funding acquisition, conceptualization, methodology, writing – review & editing. Chuan Li: investigation, data curation, writing – original draft. Jiliang Yang: formal analysis, data curation. Yefeng Liui: formal analysis, data curation. Jinpei Hei: formal analysis, software, validation. Shiqi Huang: validation. Daming Gao: supervision.

Conflicts of interest

There are no conflicts to declare.

Acknowledgements

This work was financially supported by the Natural Science Research Program of Anhui Higher Education Institutions (No. KJ2019A0679) and Discipline Construction Quality Improvement Project of Chaohu University (kj21fdzy01). The authors thank the Shiyanjia lab (**https://www.shiyanjia.com/**) for NH_3-TPD analysis.

References

1 H. W. Lee, Y. M. Kim, H. J. Jae, J. K. Jeon, S. C. Jung, S. C. Kim and Y. K. Park, *Energy Convers. Manage.*, 2016, **129**, 81–88.
2 X. Y. Li, J. LI, G. Q. Zhou, Y. Feng, Y. J. Wang, G. Yu, S. B. Deng, J. Huang and B. Wang, *Appl. Catal., A*, 2014, **469**, 490–511.
3 X. Y. Wang, X. Wang, G. X. Qin, M. Q. Chen and J. Wang, *J. Therm. Anal. Calorim.*, 2018, **132**, 1317–1323.
4 S. Ceylan and J. L. Goldfarb, *Energy Convers. Manage.*, 2015, **101**, 263–270.
5 P. S. Rezaei, H. Shafaghat and W. M. A. W. Daud, *Appl. Catal., A*, 2014, **469**, 490–511.
6 P. Pan, C. W. Hu, W. Y. Yang, T. S. Li, L. L. Dong, L. F Zhu, D. M. Tong, R. W. Qing and Y. Fan, *Bioresour. Technol.*, 2010, **101**, 4593–4599.
7 S. Thangalazhy-Gopakumar, S. Adhikari, S. A. Chattanathan and R. B. Gupta, *Bioresour. Technol.*, 2012, **118**, 150–157.
8 K. G. Wang and R. C. Brown, *Green Chem.*, 2013, **15**, 675–681.
9 Z. Y. Du, B. Hu, X. C. Ma, Y. L. Cheng, Y. H. Liu, X. Y. Lin, Y. Q. Wan, H. W. Lei, P. Chen and R. Ruan, *Bioresour. Technol.*, 2013, **130**, 777–782.
10 H. W. Lee, S. J. Choi, S. H. Park, J. K. Jeon, S. C. Jung, S. H. Joo and Y. K. Park, *Energy*, 2014, **66**, 2–6.
11 B. M. E. Chagas, C. Dorado, M. J. Serapiglia, C. A. Mullen, A. A. Boateng, M. A. F. Melo and C. H. Ataíde, *Fuel*, 2016, **179**, 124–134.
12 C. Lorenzetti, R. Conti, D. Fabbri and J. Yanik, *Fuel*, 2016, **166**, 4460452.
13 P. K. W. Likun, H. Y. Zhang, G. Ryabov, T. Vitidsant, P. Reubroycharoen and R. Xiao, *Environ. Prog. Sustainable Energy*, 2018, **37**, 1371–1379.
14 J. X. Wang, J. P. Cao, X. Y. Zhao, S. N. Liu, X. Huang, T. L. Liu and X. Y. Wei, *J. Energy Inst.*, 2020, **93**, 15–24.
15 Z. Y. Tang, W. Chen, Y. Q. Chen, J. H. Hu, H. P. Yang and H. P. Chen, *J. Anal. Appl. Pyrolysis*, 2021, **159**, 105182.
16 C. A. Mullen and A. A. Boateng, *ACS Sustain. Chem. Eng.*, 2015, **3**, 1623–1631.
17 S. Vichaphund, D. Aht-ong, V. Sricharoenchaikul and D. Atong, *Renewable Energy*, 2015, **79**, 28–37.
18 P. Li, D. Li, H. P. Yang, X. H. Wang and H. P. Chen, *Energy Fuels*, 2016, **30**, 3004–3013.
19 Y. W. Zheng, F. Wang, X. Q. Yang, Y. B. Huang, C. Liu, Z. F. Zheng and J. Y. Gu, *J. Anal. Appl. Pyrolysis*, 2017, **126**, 169–179.
20 L. Z. Sun, Z. B. Wang, L. Chen, S. X. Yang, X. P. Xie, B. F. Zhao, H. Y. Si, J. Li and D. L. Hua, *Int. J. Energy Res.*, 2021, **45**, 6032–6040.
21 M. Y. Chai, R. H. Liu and Y. F. He, *Fuel Process. Technol.*, 2020, **206**, 106458.
22 Q. F. Che, M. J. Yang, X. H. Wang, Q. Yang, L. R. Williams, H. P. Yang, J. Zou, K. Zeng, Y. J. Zhu, Y. Q. Chen and H. P. Chen, *Bioresour. Technol.*, 2019, **278**, 248–254.
23 N. Y. Yao, J. P. Cao, J. P. Zhao, Z. M. He, X. B. Feng, T. L. Liu, Z. Y. Wang and X. Y. Zhao, *Fuel*, 2022, **310**, 122437.
24 N. Shu, C. Li, D. Yellezuome, Y. K. Li and R. H. Liu, *Renewable Energy*, 2023, **209**, 569–580.
25 Y. C. Wang, Y. K. Li, C. Li, M. Y. Chai, D. Yellezuome and R. H. Liu, *J. Anal. Appl. Pyrol.*, 2022, **167**, 105692.
26 N. Shu, C. Li, M. Y. Chai, M. M. Rahman, Y. K. Li, M. Sarker and R. H. Liu, *Renewable Energy*, 2021, **175**, 936–951.
27 L. Dai, Y. P. Wang, Y. H. Liu, R. Ruan, D. L. Duan, Y. F. Zhao, T. Yu and L. Jiang, *Bioresour. Technol.*, 2019, **272**, 407–414.
28 N. H. Zainan, S. C. Srivatsa, F. Li and S. Bhattacharya, *Fuel*, 2018, **223**, 12–19.
29 S. C. Srivatsa, F. H. Li and S. Bhattacharya, *Renewable Energy*, 2019, **142**, 426–436.

30 G. X. Dai, S. R. Wang, Q. Zou and S. Q. Huang, *Fuel Process. Technol.*, 2018, **179**, 319–323.
31 F. Yang, J. G. Shao, Z. X. Yang, H. P. Yang, X. H. Wang, Z. S. Wu and H. P. Chen, *J. Anal. Appl. Pyrolysis*, 2019, **137**, 259–265.
32 K. Li, N. Shu, D. Yellezuome, M. Y. Chai, C. Li and R. H. Liu, *J. Energy Inst.*, 2021, **99**, 218–228.
33 M. Rostamizadeh and F. Yaripour, *Fuel*, 2016, **181**, 537–546.
34 J. H. Liang, H. M. Morgan, Y. J. Liu, A. P. Shi, H. W. H. Lei, H. P. Mao and Q. Bu, *J. Anal. Appl. Pyrolysis*, 2017, **128**, 324–334.
35 M. F. Yang, J. G. Shao, Z. X. Yang, H. P. Yang, X. H. Wang, Z. S. Wu and H. P. Chen, *J. Anal. Appl. Pyrolysis*, 2019, **137**, 259–265.
36 H. Chen, H. Cheng, F. Zhou, K. Q. Chen, K. Qiao, X. Y. Lu, P. K. Ouyang and J. Fu, *J. Anal. Appl. Pyrolysis*, 2018, **131**, 76–84.
37 H. Paysepar, K. T. V. Rao, Z. S. Yuan, L. Nazari, H. F. Shui and C. B. Xu, *Fuel Process. Technol.*, 2018, **178**, 362–370.
38 T. Aysu and A. Sanna, *Bioresour. Technol.*, 2015, **194**, 108–116.
39 D. J. Mihalcik, C. A. Mullen and A. A. Boateng, *J. Anal. Appl. Pyrolysis*, 2011, **92**, 224–232.
40 K. G. Wang, K. H. Kim and R. C. Brown, *Green Chem.*, 2014, **16**, 727–735.
41 H. Tian, Y. Y. Wei, Z. J. Huang, Y. Q. Chen, O. Tursunov, S. Cheng, H. P. Yang and Y. Yang, *Fuel*, 2023, **333**, 126215.
42 B. Gu, J. P. Cao, F. Wei, X. Y. Zhao, X. Y. Ren, C. Zhu, Z. X. Guo, J. Bai, W. Z. Shen and X. Y. Wei, *Fuel*, 2019, **244**, 151–158.
43 S. Kelkar, C. M. Saffron, Z. Li, S. S. Kim, T. J. Pinnavaia, D. J. Miller and R. Kriegel, *Green Chem.*, 2014, **16**, 803–812.
44 J. Socci, A. Saraeian, S. D. Stefanidis, S. W. Banks, B. H. Shanks and T. Bridgwater, *J. Anal. Appl. Pyrolysis*, 2022, **162**, 104710.
45 E. B. Hassan, I. Elsayed and A. Eseyin, *Fuel*, 2016, **174**, 317–324.
46 H. Zhou, C. F. Wu, J. A. Onwudili, A. H. Meng, Y. G. Zhang and P. T. Williams, *Energy Fuels*, 2014, **28**, 6371–6379.
47 A. G. Gayubo, A. T. Aguayo, A. Atutxa and J. Bilbao, *Energy Fuels*, 2004, **18**, 1640–1647.
48 M. Sanchez, J. Menendez, A. Domínguez, J. Pis, O. Martínez, L. Calvo and P. Bernad, *Biomass Bioenergy*, 2009, **33**, 933–940.
49 Z. Y. Du, X. C. Ma, Y. Li, P. Chen, Y. H. Liu, X. Y. Lin, H. W. Lei and R. Ruan, *Bioresour. Technol.*, 2013, **139**, 397–401.
50 X. Wang, L. L. Sheng and X. Y. Yang, *Bioresour. Technol.*, 2017, **229**, 119–125.
51 R. Gautam and R. Vinu, *React. Chem. Eng.*, 2019, **4**, 278–297.
52 T. R. Carlson, J. Jae, Y. C. Lin, G. A. Tompsett and G. W. Huber, *J. Catal.*, 2010, **270**, 110–124.
53 P. Y. Qi, G. Z. Changa, H. C. Wang, X. L. Zhang and Q. J. Guo, *J. Anal. Appl. Pyrolysis*, 2018, **136**, 178–185.
54 A. M. M. Araújo, R. O. Lima, A. D. Gondim, J. Diniz, L. D. Souza and A. S. Araujo, *Renewable Energy*, 2017, **101**, 900–906.
55 H. Chen, Q. F. Wang, X. W. Zhang and L. Wang, *Appl. Catal. B Environ.*, 2015, **167**, 327–334.
56 W. Chen, H. P. Yang, Y. Q. Chen, M. W. Xia, X. Chen and H. P. Chen, *Environ. Sci. Technol.*, 2017, **51**, 6570–6579.
57 B. Gu, J. P. Cao, F. Wei, X. Y. Zhao, X. Y. Ren, C. Zhu, Z. X. Guo, J. Bai, W. Z. Shen and X. Y. Wei, *Fuel*, 2019, **244**, 151–158.